



## Research Article

# Design of a three-nozzle for air spraying based on jet interference effect and numerical study of spraying process



Xiao-Peng Xie<sup>1</sup> · Yin-An Wang<sup>1</sup>

Received: 1 January 2022 / Accepted: 25 April 2022

Published online: 16 May 2022

© The Author(s) 2022 [OPEN](#)

### Abstract

Due to the problems of many round-trip time and low spraying efficiency when using single-nozzle, a three-nozzle structure is studied in this paper. The spraying process is numerically simulated by the method of computational fluid dynamics. The discrete phase model is used to predict the trajectory of droplets. The interference flow field is formed due to the entrainment of jet. Paint droplets are transported to the target under the action of gas flow field. The geometry of three-nozzle has a significant influence on the characteristics of the interference flow field. The influence of different distance ( $L$ ) and axis angle ( $\theta$ ) between two adjacent paint holes on the interference gas flow field and coating thickness distribution are analyzed by changing the structure of three-nozzle. Numerical simulation results show that small  $L$  and  $\theta$  result in strong interference effect, while the paint is mainly concentrated in the central region of the target, which is easy to cause overspray. With the gradual increase of  $L$  and  $\theta$ , the strength of interference gradually decreases and the paint gradually spreads to both sides. However, the strength of interference would become very small when  $L$  and  $\theta$  get too large, which is easy to cause an uneven coating film. According to the numerical simulation results, the best spraying effect can be obtained when  $L=40$  mm and  $\theta=30^\circ$ . Compared with single-nozzle and double-nozzle, the effective coating film width of three-nozzle has increased by 414.3% and 176.9%, respectively, which improves the spraying efficiency.

### Article Highlights

- For the problem of low efficiency of single nozzle, this paper studies a three-nozzle based on jet interference effect.
- The coating film thickness distribution model is established based on numerical simulation, which avoids expensive and time-consuming experiments.
- Compared with single-nozzle and double-nozzle, the effective film width of three-nozzle has increased by 414.3% and 176.9%, respectively, which improved the spraying efficiency

**Keywords** Three-nozzle · Numerical simulation · Entrainment · Interference gas flow field · Coating film thickness distribution

✉ Yin-An Wang, 201510100307@mail.scut.edu.cn; Xiao-Peng Xie, xiexp@scut.edu.cn | <sup>1</sup>Dongguan City College, 1 Wenchang Road, Dongguan 523419, China.



SN Applied Sciences

(2022) 4:177

| <https://doi.org/10.1007/s42452-022-05046-4>

SN Applied Sciences  
A **SPRINGER NATURE** journal

## 1 Introduction

Air spray guns were widely used in many industries such as automobile, aero-space, aircraft, ship, and furniture, due to its good atomization performance [1–3]. Robot spraying has attracted more and more attention with the development of robot technology. When using robot spraying, the establishment of coating film thickness distribution model and the planning of spraying trajectory are still difficult problems to be solved. Inaccurate coating film thickness distribution model and inappropriate spraying trajectory will result in poor spraying quality and unqualified products. There are two main methods of spraying trajectory planning of spraying robot, teaching programming and off-line programming. The method of teaching programming has low flexibility. The quality of spraying depends on workers' experience, which is difficult to meet the requirements. In order to solve these problems, many researchers began to use off-line programming to plan the spraying trajectory of robot [4–7].

The establishment of coating accumulation model is an important module of off-line programming technology of spraying robot. There are mainly two methods to establish coating accumulation model: fitting function method based on experimental measurement and numerical simulation method based on CFD [8]. The first method mainly includes infinite range model and limited range model. The former includes Cauchy distribution model [9], Gaussian distribution model [10] and so on. The later includes parabolic distribution model [11], piecewise function distribution model [12],  $\beta$  distribution model [13], ellipse dual- $\beta$  distribution model [14] and so on. The disadvantages of the fitting function method based on experimental measurements are: (1) over-reliance on expensive and complex experiments; (2) once the spraying parameters are changed, the model will fail, because the model is established for special spraying parameters; (3) the spraying process and formation mechanism of coatings film cannot be analyzed by this method.

With the development of CFD technology, some scholars began to use numerical simulation methods to establish coating accumulation models. The spraying process of air spray guns can be divided into three parts: paint's atomization process, droplets' transportation process, droplets' deposition process. This method describes the spray flow field as two-phase flow of air and paint droplets. Euler-Euler and Euler-Lagrangian are two commonly used methods to describe the two-phase flow field of spraying process.

Euler-Euler method treats both air and droplets as continuous phases, and both gas and droplets are

calculated in Euler coordinate system. Chen et al. [15] used Euler-Euler method to simulate the spraying process of air spray gun and analyzed the coating film thickness distribution. Chen et al. [16] established the coating accumulation model of air spray gun by using the dynamic grid. Since Euler-Euler method does not need to track a large number of droplets, it can save computing resources. However, Euler-Euler method is not applicable when the volume fraction of paint is small.

Euler-Lagrangian method treats air paint droplets as continuous phase and discrete phase respectively. The continuous phase is calculated in Euler coordinate system and the discrete phase is calculated in Lagrangian coordinate system. The research on numerical simulation of air spraying process using Euler-Lagrangian method mainly focuses on droplet size distribution, air flow field, droplet trajectory, and coating thickness distribution. Ye et al. [17] and Domnick et al. [18, 19] obtained the initial conditions for calculating the flow field using an experiment-based method. They measured the size and velocity of paint droplet under the nozzle with the help of phase doppler analyzer (PDA), and set the initial conditions of discrete phase directly close to the nozzle. However, once the spraying parameters of this method were changed, time-consuming and expensive experiments need to be repeated. Fogliati et al. [20] used VOF model to simulate the paint jet at the outlet of the spray gun and estimated the initial conditions of the droplets. However, this method does not predict the secondary breakup of paint droplets.

At present, the research about air spray gun was mostly focused on the single-nozzle. Numerical simulation of single-nozzle and double-nozzle was studied in our previous work [21, 22]. Single-nozzle has the disadvantages of many round-trip times and low spraying efficiency when spraying large target surfaces. Double-nozzle could reduce the round-trip times and spraying time. In order to obtain a higher spraying efficiency, a new three-nozzle structure is studied in this paper. Negative pressure is generated between the jets due to the entrainment effect of jets, which causes the jets to close together and form an interference air flow field. Paint droplets are transported to the workpiece surface under the action of air flow to form a coating film. The interference gas flow field of three-nozzle was numerically simulated by changing the values of  $L$  and  $\theta$ . In addition, the influence of three-nozzle structure on coating film thickness distribution was analyzed.

The following section presents the preparation for the numerical simulation of the three-nozzle, including the geometry of three-nozzle, generation of grids for computational domain and description of the calculation methods and initial conditions. This section is followed by the results and discussion, which reports the simulation results

of velocity field and coating film thickness distribution. The last section is the conclusions.

## 2 Computational model

### 2.1 Geometry of three-nozzle

The geometry of three-nozzle studied in this paper is shown in Fig. 1. There are three lines of holes on the three-nozzle: each line has a circular paint hole, an annular atomizing air hole, four assisting air holes and four shaping air holes. The diameter of paint hole is 1.5 mm. The outer side of paint hole is an annular atomizing air hole. The outer and inner diameters are 2.5 mm and 2 mm respectively. The role of atomizing air flow is to atomize the paint into droplets and transport them to the workpiece surface. Both sides of atomizing air hole are assisting air hole. The diameter of assisting air hole is 0.5 mm. The assisting air flow can not only control the expansion speed of gas flow field, but also keep the surface of three-nozzle clean. 12 shaping air holes are symmetrically distributed on both sides of three-nozzle. The diameter of shaping air hole is 1.5 mm. The role of shaping airflow is to change the shape of gas flow field and obtain coating film with different shapes.  $L$  and  $\theta$  represent the distance and axis angle between two adjacent paint holes respectively.

The spraying schematic diagram and coordinate system definition of three-nozzle are shown in Fig. 2. The shape of coating film is elliptical under the action of shaping air flow. The intersection of the center axis of three-nozzle and the target surface is the origin of coordinate system. The X-axis and Y-axis are parallel to the short and long axis of elliptical coating film. The Z-axis is along the center axis of three-nozzle.

### 2.2 Computational domain and grid

ICEM software was used to create the computational domain and generate unstructured grid for three-nozzle.

Fig. 1 Geometry of three-nozzle

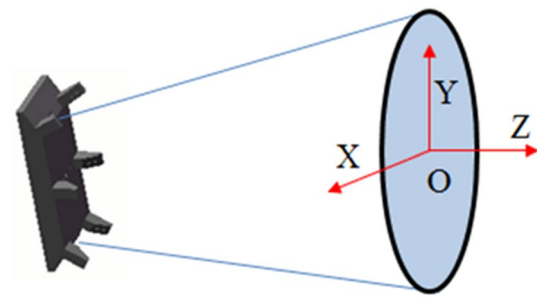
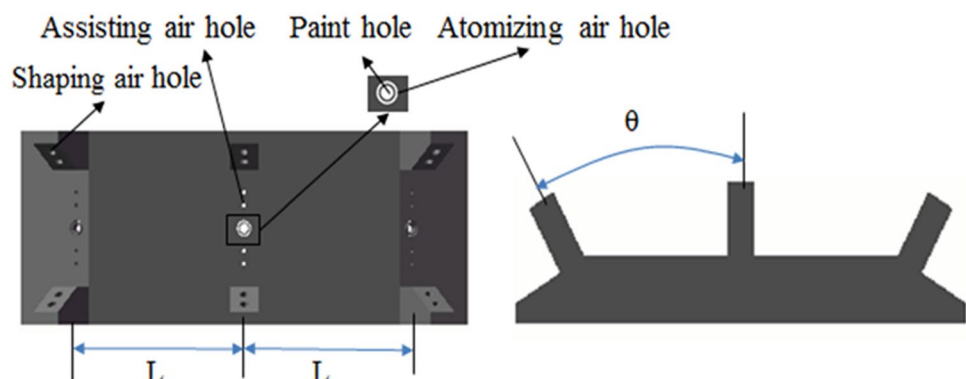
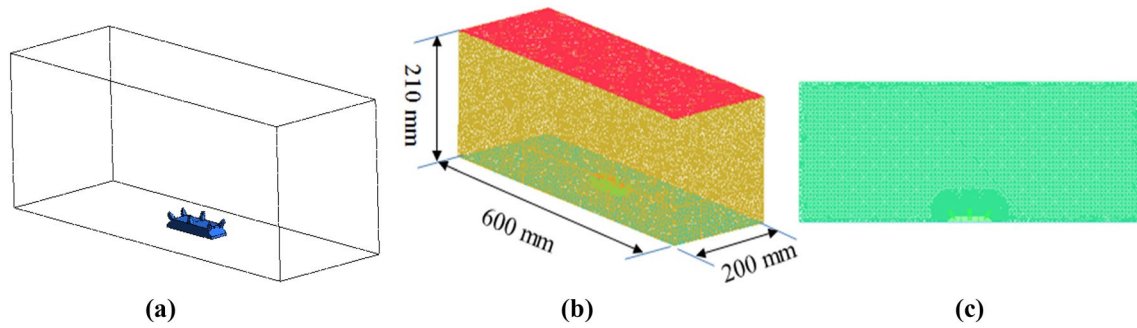


Fig. 2 Definition of coordinate system

Figure 3 shows the computational domain and unstructured grid. Considering the complex structure of three-nozzle and the area of elliptical coating film, the size of computational domain was set to  $600 \times 200 \times 210 \text{ mm}^3$ . Three-nozzle is located in the center of lower surface. The upper surface is the target. The spraying distance is 200 mm. Due to the complex structure of three-nozzle and fast airflow velocity in the region near the nozzle, local grid refinement method was applied in this paper. In order to accurately describe the effect of air flow on paint droplets and improve the calculation accuracy, a higher grid resolution was adopted in the region near the nozzle. In order to increase the calculation speed and save computing resources, a lower grid resolution was used in the region far from the nozzle.

### 2.3 Methods and initial conditions

The spraying process of three-nozzle can be regarded as a gas-liquid two-phase flow field. In this paper, Euler-Lagrange method was used to model the two-phase flow field. The software platform for simulation is ANSYS-Fluent. The finite volume method was used to simulate the spraying process. Coupled solver and second-order upwind scheme were used to calculate the three-dimensional compressible airflow. The standard  $k-\epsilon$  model was used to calculate the turbulent transport



**Fig. 3** Computational domain and grid: **a** calculation domain; **b** overall unstructured grid; **c** grid at section  $x=0$

process. DPM model was used to track the trajectory of discrete phase. TAB model was used to describe the secondary breakup process of paint droplets. The turbulent diffusion of paint droplets in the gas flow field can be simulated by calculating the trajectories of a large number of representative particles with the help of stochastic tracking model. Euler wall film model was used to calculate the coating film thickness distribution on the workpiece.

The motion equation of discrete phase is:

$$\frac{du_p}{dt} = F_D(u - u_p) + F_G \tag{1}$$

in which  $F_D(u - u_p)$  is the drag force;  $F_G$  is the gravity force;  $u_p$  is the velocity of droplet;  $u$  is the instantaneous velocity of air; which is obtained by adding the local average velocity and the pulsating velocity caused by turbulence.

Since the density of air is much smaller than that of droplets, the virtual force and Saffman force can be ignored. Since the mass flow of paint is generally small, the interaction force between droplets can be ignored. The droplet trajectory can be obtained by integrating the motion equation of discrete phase.

Due to the complexity of atomization, many researchers have not studied the process of jet atomization. Rather, it is assumed that the paint has been completely atomized at a position very close to the nozzle. The velocity and size distribution of droplets are obtained through experiments. In order to avoid dependence on experiment, simplified inlet boundary conditions are used for both continuous and discrete phase. The discrete phase is directly added at the position of paint hole. All paint holes were set as mass inlets, with a mass flow rate of  $1 \times 10^{-3}$  kg/s and an initial velocity of 50 m/s [23]. Atomizing air holes, shaping air holes, and assisting air holes were set as pressure inlets. The surface of three-nozzle and target surface were set as walls. The other boundaries were set as pressure outlets, with a static

**Table 1** Application parameters used in the simulations

Atomizing air	Shaping air (MPa)	Assisting air (MPa)	Liquid flow rate (kg/s)
0.15 MPa	0.07	0.15	0.0012

**Table 2** The properties of the liquid and gas

Materials	Density (kg/m <sup>3</sup> )	Surface tension (mN/m)	Viscosity (Pa·s)
Paint	1200	71.9	0.065
Air	1.29	–	$1.8 \times 10^{-5}$

**Table 3** Values of L and  $\theta$

Variables	values
L	20, 30, 40, 50 mm
$\theta$	10, 20, 30, 40°

pressure of 0 MPa. The main parameters and material properties of three-nozzle are shown in Tables 1 and 2.

### 3 Simulation results and discussion

#### 3.1 Structure parameters of three-Nozzle

This paper studied a new three-nozzle. By setting different values of L and  $\theta$ , the influence of the structure of three-nozzle on the interference gas flow field and coating film thickness distribution was analyzed. The values of L and  $\theta$  are shown in Table 3.

#### 3.2 Simulation results of velocity field

Firstly, the influence of  $\theta$  on gas flow field was analyzed. Set the value of L to 40 mm and keep it unchanged. Set

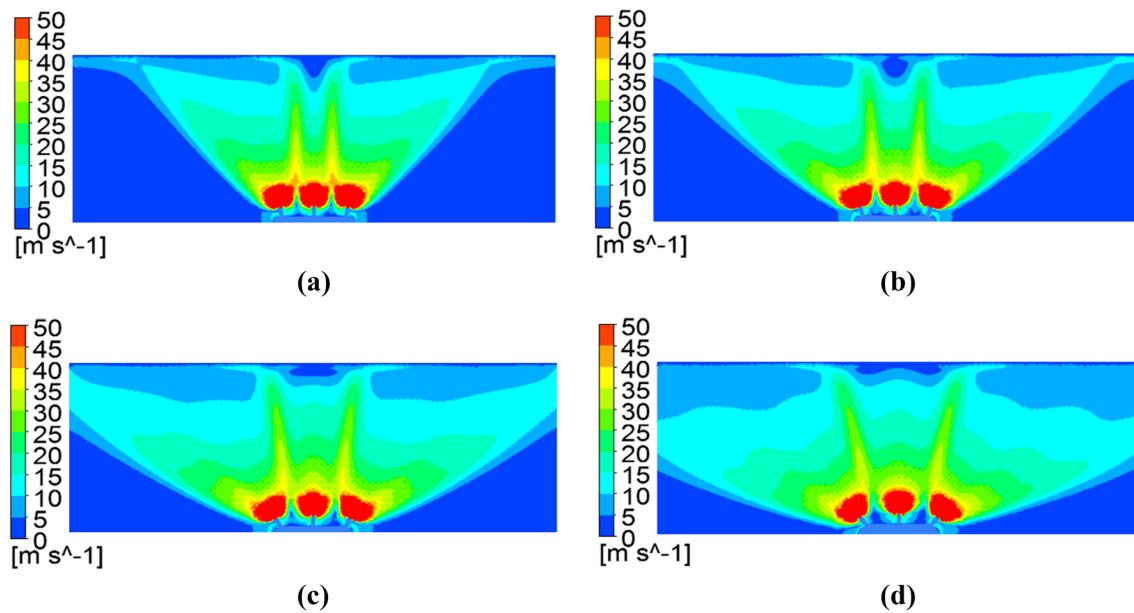


**Fig. 4** Velocity contours at section  $X=0$  for different  $\theta$  when  $L=40$  mm: **a**  $\theta=10^\circ$ ; **b**  $\theta=20^\circ$ ; **c**  $\theta=30^\circ$ ; **d**  $\theta=40^\circ$

the value of  $\theta$  to  $10^\circ$ ,  $20^\circ$ ,  $30^\circ$ ,  $40^\circ$  respectively. Figure 4 shows the gas velocity contours at section  $X=0$  for different  $\theta$ . In order to facilitate viewing the entire gas velocity flow field, set the maximum displayed velocity to 50 m/s. It can be seen from the figure that the gas velocity near the nozzle is big. With the increase of the distance from the nozzle, the gas velocity gradually decreases, which is due to the entrainment effect of jets. Due to the momentum exchange between the jets and the surrounding static air, the gas velocity decreases gradually along the Z-axis. A negative pressure zone was formed between two adjacent jets, due to the entrainment effect of jet. Two adjacent jets attract each other and merge into one jet, and finally form an interference gas flow field. The gas velocity in the middle region of two adjacent jets is relatively large. When  $\theta=10^\circ$ , the strength of interference effect between jets is the largest, and the expansion width of gas flow field along the Y-axis is the smallest. With the value of  $\theta$  increases, the strength of interference effect gradually decreases, and the expansion width of gas flow field along the Y-axis gradually increases.

Then, the influence of  $L$  on gas flow field was analyzed. Set the value of  $\theta$  to  $10^\circ$  and keep it unchanged. Set the value of  $L$  to 20 mm, 30 mm, 40 mm, and 50 mm respectively. The spraying process of three-nozzle was numerically simulated. Figure 5 shows the gas velocity contours at section  $X=0$  for different  $L$ . Set the maximum displayed velocity to 50 m/s. It can be seen from the figure that there is a big gas velocity near the nozzle. With the increase of the distance from the nozzle, the gas velocity gradually decreases, which is due to the entrainment effect of jets.

Due to the momentum exchange between the jets and the surrounding static air, the gas velocity decreases gradually along the Z-axis. A negative pressure zone was formed between two adjacent jets, due to the entrainment effect of jet. Two adjacent jets attract each other and merge into one jet, and finally form an interference gas flow field. The gas velocity in the middle region of two adjacent jets is relatively large. When  $L=20$  mm, the strength of interference effect between jets is the largest, and the expansion width of gas flow field along the Y-axis is the smallest. As the value of  $L$  increases, the strength of interference effect gradually decreases, and the expansion width of gas flow field along the Y-axis gradually increases.

The interference gas flow field was formed due to the entrainment effect. The influence of  $L$  and  $\theta$  on the interference gas flow field is similar. When the values of  $L$  and  $\theta$  are small, the intensity of interference between jets is small. With the values of  $L$  and  $\theta$  increase, the strength of interference effect gradually decreases. The interference gas flow field has a great influence on the droplet trajectory. Therefore, different coating film thickness distribution can be obtained by adjusting the values of  $L$  and  $\theta$ .

### 3.3 Simulation results of coating thickness distribution

Coating film thickness contours with different values of  $L$  and  $\theta$  are shown in Figs. 6, 7, 8, and 9. It can be seen that  $L$  and  $\theta$  have similar effects on the coating film thickness distribution. When the values of  $L$  and  $\theta$  are small, the shape of coating film is diamond, and the paint is



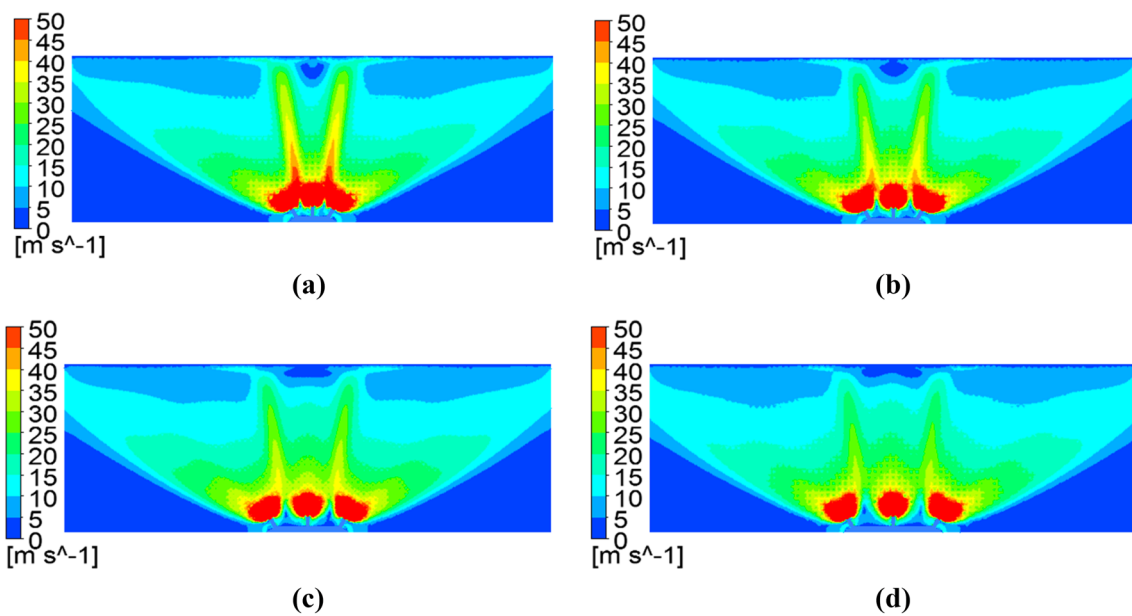
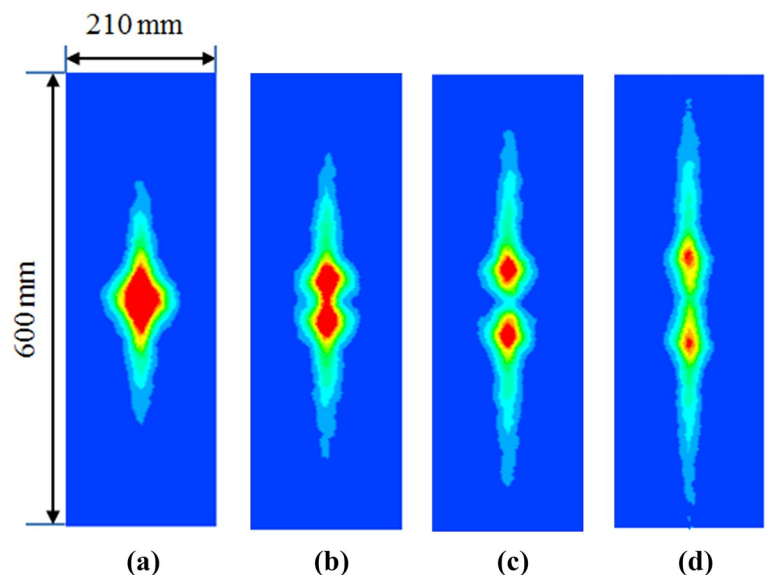


Fig. 5 Velocity contours at section  $X=0$  for different  $L$  when  $\theta=30^\circ$ : **a**  $L=20$  mm; **b**  $L=30$  mm; **c**  $L=40$  mm; **d**  $L=50$  mm

Fig. 6 Coating thickness contours for different  $\theta$  when  $L=20$  mm: **a**  $\theta=10^\circ$ ; **b**  $\theta=20^\circ$ ; **c**  $\theta=30^\circ$ ; **d**  $\theta=40^\circ$

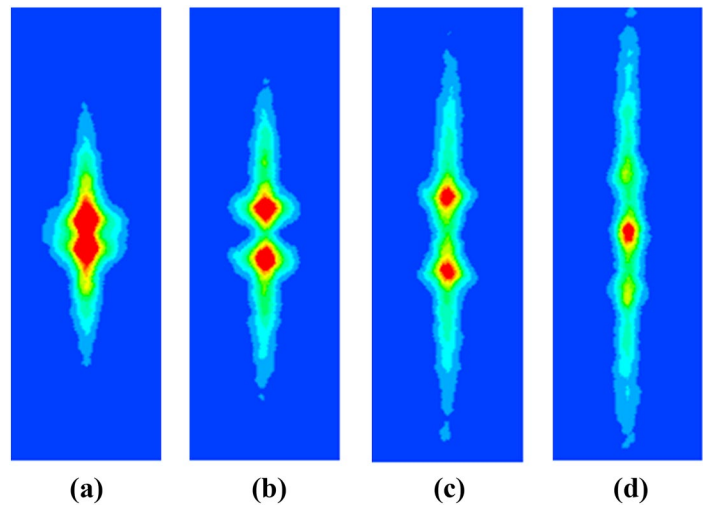


concentrated in the center region of target surface, which is easy to cause overspray. With the values of  $L$  and  $\theta$  increase, the expansion width of coating film along the  $Y$ -axis gradually increases. The shape of coating film gradually changes from a rhombus to an "8", and then to an approximate ellipse. When the values of  $L$  and  $\theta$  are small, the strength of interference effect between jets is greater. The three jets attract each other and merge into one jet, causing the coating film to expand along the  $X$ -axis. With the values of  $L$  and  $\theta$  gradually increase, the strength of interference between jets gradually decreases. The jet in the middle is attracted to the jets on both sides, and the

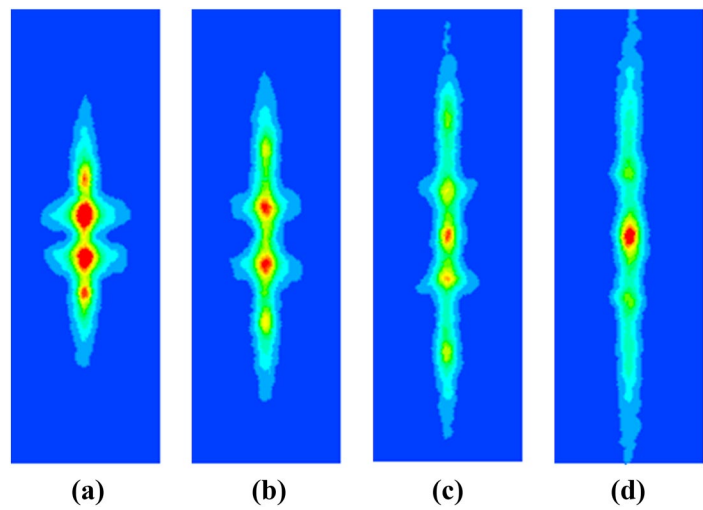
three jets gradually change into two jets, resulting in an "8"- shape coating film. With the values of  $L$  and  $\theta$  continue to increase, the strength of interference effect between jets continues to decrease.

Figure 10 shows the coating thickness profiles along the  $Y$ -axis for different values of  $L$  and  $\theta$ . It can be seen that the coating thickness profiles has only one peak when the values of  $L$  and  $\theta$  are small. The coating thickness profiles are convex-shape lines with a larger height in the middle region and a smaller height on both sides. The paint is concentrated in the central region. With the values of  $L$  and  $\theta$  increase, the coating thickness profiles

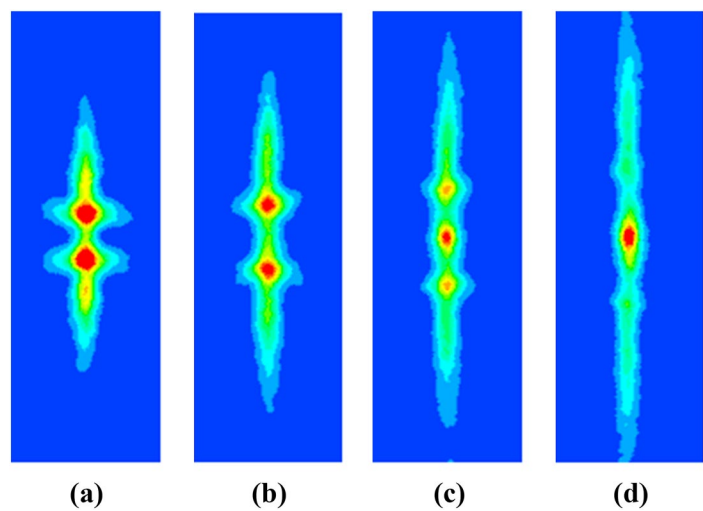
**Fig. 7** Coating thickness contours for different  $\theta$  when  $L=30$  mm: **a**  $\theta=10^\circ$ ; **b**  $\theta=20^\circ$ ; **c**  $\theta=30^\circ$ ; **d**  $\theta=40^\circ$



**Fig. 8** Coating thickness contours for different  $\theta$  when  $L=40$  mm: **a**  $\theta=10^\circ$ ; **b**  $\theta=20^\circ$ ; **c**  $\theta=30^\circ$ ; **d**  $\theta=40^\circ$



**Fig. 9** Coating thickness contours for different  $\theta$  when  $L=50$  mm: **a**  $\theta=10^\circ$ ; **b**  $\theta=20^\circ$ ; **c**  $\theta=30^\circ$ ; **d**  $\theta=40^\circ$



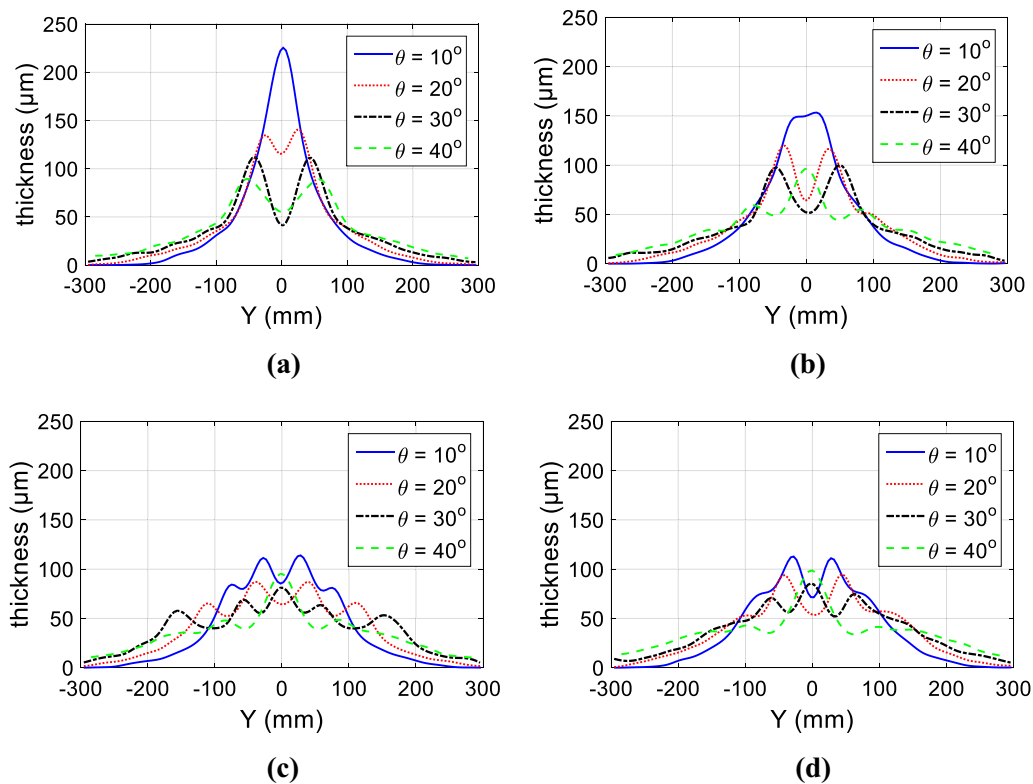


Fig. 10 Coating thickness profiles: **a** L=20 mm; **b** L=30 mm; **c** L=40 mm; **d** L=50 mm

gradually becomes concave-shape lines with a smaller height in the middle region and a larger height on both sides. The coating thickness profiles have two peaks. With the values of L and  $\theta$  increase, the expansion width of coating film along the Y-axis gradually increases, and the uniformity of coating film gradually becomes better. However, the coating thickness profiles will turn into convex-shape lines with a larger height in the middle region and a smaller height on both sides. According to the simulation results, a more uniform coating film can be obtained when L = 40 mm and  $\theta = 30^\circ$ , and the spraying effect is best at this point.

### 3.4 Comparison of three-nozzle, double-nozzle and single-nozzle

The same boundary conditions and initial conditions were set respectively. The spraying process of single-nozzle, double-nozzle, and three-nozzle was numerically simulated. Refer to Tables 1 and 2 in Sect. 2.3 for spraying parameters. The coating thickness contour of three-nozzle when L=40 mm and  $\theta = 30^\circ$  is shown in Fig. 11a. The coating thickness contour of double-nozzle is shown in Fig. 11b. The values of the distance between the centers of two paint holes and the angle between the two paint holes are 30 mm and  $10^\circ$  respectively. According to the

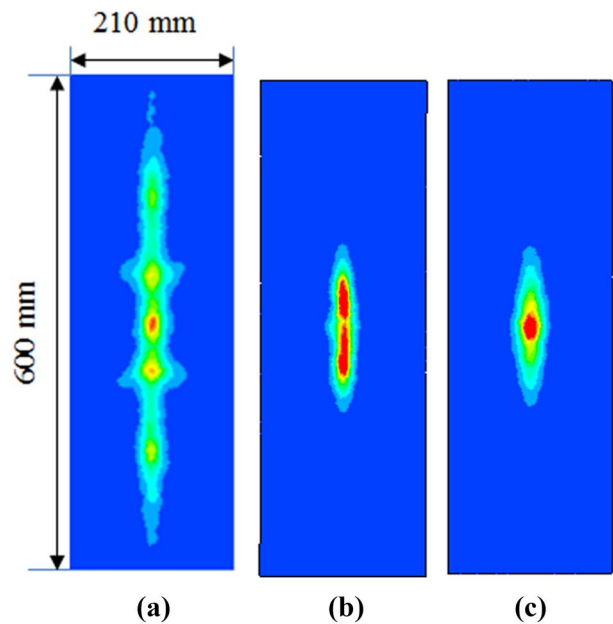
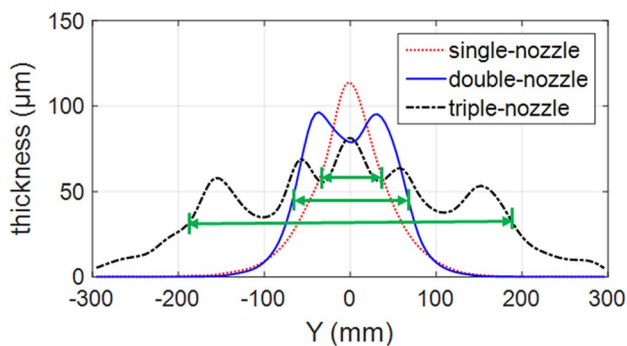


Fig. 11 Coating film thickness distribution contours: **a** three-nozzle; **b** double-nozzle; **c** single-nozzle [21, 22]

previous research [21, 22], the spraying effect is the best at this point. The coating thickness contour of single-nozzle is shown in Fig. 11c.





**Fig. 12** Comparison of coating thickness distribution profiles of three-nozzle, double-nozzle and single-nozzle along Y-axis [21, 22]

The comparison of coating thickness profiles of three-nozzle, double-nozzle, and single-nozzle along the Y-axis is shown in Fig. 12. It can be seen that the spraying effect of three-nozzle is the best compared with double-nozzle and single-nozzle. A more uniform coating film can be obtained through three-nozzle. Define the effective coating thickness as half the maximum coating thickness. The effective width of coating film of three-nozzle, double-nozzle, and single-nozzle are about 360 mm, 130 mm, and 70 mm, respectively. Compared with double-nozzle and single-nozzle, the effective width of coating film of three-nozzle is increased by 414.3% and 176.9%, respectively. Therefore, the three-nozzle can effectively improve the spraying efficiency.

## 4 Conclusions

This paper studied a new three-nozzle structure applied to air spraying. The spraying process of three-nozzle was numerically simulated using ANSYS-Fluent software, and the distribution of gas flow field and coating film thickness on the target were obtained. Due to the entrainment effect of jets, negative pressure was formed in the region between adjacent jets. Under the action of pressure difference, the two jets attracted and merged with each other to form an interference gas flow field.

The influence of  $L$  and  $\theta$  on the interference gas flow field is similar. When the values of  $L$  and  $\theta$  are the smallest, the strength of interference effect between jets is the largest, the expansion width of gas flow field along Y-axis is the smallest. As the values of  $L$  and  $\theta$  increase, the strength of interference effect between jets gradually decreases, and the expansion width of gas flow field along Y-axis gradually increases. Since the interference gas flow field has a significant effect on the droplet trajectory and coating film thickness distribution, different coating film

thickness distribution can be obtained by adjusting the values of  $L$  and  $\theta$ .

The influence of  $L$  and  $\theta$  on the coating film thickness distribution is similar. When the values of  $L$  and  $\theta$  are small, the shape of coating film is diamond, and the paint is concentrated in the center region of target surface, which is easy to cause overspray. As the values of  $L$  and  $\theta$  increase, the expansion width of coating film along Y-axis gradually increases, and the shape of coating film gradually changes from a rhombus to an "8" and finally becomes an approximate ellipse. According to the simulation results, a more uniform coating film can be obtained when  $L=40$  mm and  $\theta=30^\circ$ , and the spraying effect is best at this point. Compared with single-nozzle and double-nozzle, the effective coating width obtained by three-nozzle has increased by 414.3% and 176.9% respectively. Therefore, the three-nozzle can effectively improve the spraying efficiency.

**Funding** This work was supported by the Major Science and Technology Cultivation Project of City College of Dongguan University of Technology (Grant No. 2018YZD001Z).

**Data availability** All data used in the research are available upon request.

## Declarations

**Conflict of interest** The authors declare that there is no conflict of interest.

**Open Access** This article is licensed under a Creative Commons Attribution 4.0 International License, which permits use, sharing, adaptation, distribution and reproduction in any medium or format, as long as you give appropriate credit to the original author(s) and the source, provide a link to the Creative Commons licence, and indicate if changes were made. The images or other third party material in this article are included in the article's Creative Commons licence, unless indicated otherwise in a credit line to the material. If material is not included in the article's Creative Commons licence and your intended use is not permitted by statutory regulation or exceeds the permitted use, you will need to obtain permission directly from the copyright holder. To view a copy of this licence, visit <http://creativecommons.org/licenses/by/4.0/>.

## References

1. Andulkar MV, Chiddarwar SS, Marathe AS (2015) Novel integrated offline trajectory generation approach for robot assisted spray painting operation. *J Manuf Syst* 37:201–216. <https://doi.org/10.1016/j.jmsy.2015.03.006>
2. Chen H, Xi N (2008) Automated tool trajectory planning of industrial robots for painting composite surfaces. *Int J Adv Manuf Technol* 35:680–696. <https://doi.org/10.1007/s00170-006-0746-5>

3. Chen W, Chen Y, Li B, Zhang W, Chen K (2016) Design of redundant robot painting system for long non-regular duct. *Ind Robot* 43:58–64. <https://doi.org/10.1108/ir-06-2015-0113>
4. Guan L, Chen L (2019) Trajectory planning method based on transitional segment optimization of spray painting robot on complex-free surface. *Ind Robot* 46:31–43. <https://doi.org/10.1108/ir-02-2018-0033>
5. Park K, Jeon D (2018) Optimization of tool path pitch of spray painting robots for automotive painting quality. *Int J Control Autom Syst* 16:2832–2838. <https://doi.org/10.1007/s12555-018-0055-4>
6. Chen H, Xi N (2012) Automated robot tool trajectory connection for spray forming process. *J Manuf Sci Eng Trans ASME* 134:9. <https://doi.org/10.1115/1.4005798>
7. Zhang YJ, Li WB, Zhang C, Liao HL, Zhang YC, Deng SH (2019) A spherical surface coating thickness model for a robotized thermal spray system. *Robot Comput Integr Manuf* 59:297–304. <https://doi.org/10.1016/j.rcim.2019.05.003>
8. Chen Y, Chen WZ, Li B, Zhang G, Zhang WM (2017) Paint thickness simulation for painting robot trajectory planning: a review. *Ind Robot* 44:629–638. <https://doi.org/10.1108/ir-07-2016-0205>
9. Antonio JK (1994) Optimal trajectory planning for spray coating. In: *Proceedings of the 1994 IEEE international conference on robotics and automation*, pp 2570–2577. <https://doi.org/10.1109/robot.1994.351125>
10. Freund E, Rokossa D, Rossmann J (1998) Process-oriented approach to an efficient off-line programming of industrial robots. In: *Ilecon '98—proceedings of the 24th annual conference of the IEEE industrial electronics society*. IEEE, New York, pp 208–213. <https://doi.org/10.1109/IECON.1998.723992>
11. Chen HP, Xi N, Sheng WH, Chen MF (2005) General framework of optimal tool trajectory planning for free-form surfaces in surface manufacturing. *J Manuf Sci Eng Trans* 127:49–59. <https://doi.org/10.1115/1.1828057>
12. Klein A (1987) CAD-based off-line programming of painting robots. *Robotica (UK)* 5:267–271. <https://doi.org/10.1017/s0263574700016283>
13. Arıkan MAS, Balkan T (2006) Modeling of paint flow rate flux for elliptical paint sprays by using experimental paint thickness distributions. *Ind Robot* 33:60–66. <https://doi.org/10.1108/01439910610638243>
14. Zhang Y, Huang Y, Gao F, Wang W (2006) New model for air spray gun of robotic spray-painting. *Chin J Mech Eng (China)* 42:226–233
15. Chen Y, He S, Zhang G, Chen W (2015) Two-fluid model simulation of paint deposition on flat wall in an air spray process. *J Logist Eng Univ* 31:82–86
16. Chen WZ, Chen Y, Zhang WM, He SW, Li B, Jiang JZ (2019) Paint thickness simulation for robotic painting of curved surfaces based on Euler–Euler approach. *J Braz Soc Mech Sci Eng* 41:9. <https://doi.org/10.1007/s40430-019-1651-9>
17. Ye QY, Pulli K (2017) Numerical and experimental investigation on the spray coating process using a pneumatic atomizer: influences of operating conditions and target geometries. *Coatings* 7:10. <https://doi.org/10.3390/coatings7010013>
18. Domnick J, Scheibe A, Ye QY (2005) The simulation of the electrostatic spray painting process with high-speed rotary bell atomizers. Part I: direct charging. *Part Part Syst Charact* 22:141–150. <https://doi.org/10.1002/ppsc.200400968>
19. Domnick J, Scheibe A, Ye QY (2007) The simulation of electrostatic spray painting process with high-speed rotary bell atomizers. Part II: external charging. *Part Part Syst Charact* 23:408–416. <https://doi.org/10.1002/ppsc.200601018>
20. Fogliati M, Fontana D, Garbero M, Vanni M, Baldi G, Donde R (2006) CFD simulation of paint deposition in an air spray process. *JCT Res* 3:117–125. <https://doi.org/10.1007/s11998-006-0014-5>
21. Xie X, Wang Y (2019) Research on distribution properties of coating film thickness from air spraying gun-based on numerical simulation. *Coatings* 9:721. <https://doi.org/10.3390/coatings9110721>
22. Wang YA, Xie XP, Lu XH (2020) Design of a double-nozzle air spray gun and numerical research in the interference spray flow field. *Coatings* 10:475. <https://doi.org/10.3390/coatings10050475>
23. Li W, Qian L, Song S, Zhong X (2019) Numerical study on the influence of shaping air holes on atomization performance in pneumatic atomizers. *Coatings* 9:410. <https://doi.org/10.3390/coatings9070410>

**Publisher's Note** Springer Nature remains neutral with regard to jurisdictional claims in published maps and institutional affiliations.